Microporous and Mesoporous Materials 204 (2015) 242–250

Contents lists available at ScienceDirect

Microporous and Mesoporous Materials

journal homepage: www.elsevier.com/locate/micromeso

# Hierarchical embedding of micro-mesoporous MIL-101(Cr) in macroporous poly(2-hydroxyethyl methacrylate) high internal phase emulsions with monolithic shape for vapor adsorption applications

Martin Wickenheisser, Christoph Janiak *

*Institut für Anorganische Chemie und Strukturchemie I, Universitätsstraße 1, 40225 Düsseldorf, Germany*

ARTICLE INFO

*Article history:*
Received 3 September 2014
Received in revised form 14 October 2014
Accepted 22 November 2014
Available online 4 December 2014

*Keywords:*
Metal-organic framework
Hierarchical porosity
High internal phase emulsion (HIPE)
Monoliths
Heat transformation

ABSTRACT

Shaping metal-organic frameworks (MOFs), normally obtained as powders or microcrystals, e.g., into monoliths is one indispensable factor for potential applications of MOFs. MIL-101(Cr) as a water stable micro- and mesoporous network was successfully embedded into a macroporous and monolithic oil–water (o/w) high internal phase emulsion (HIPE) foam, based on crosslinked poly(2-hydroxyethyl methacrylate). These hierarchical and mechanically stable monolithic composite materials with up to 59 wt% of MIL-101(Cr) show higher methanol and water vapor uptake capacities compared to the pure HIPE.



## 1. Introduction

MOFs (metal-organic framework) are three-dimensional permanently porous networks based on metal ions or metal clusters, connected by organic ligands [1,2]. Metal organic frameworks have uniform micropore structures with high surface areas and large pore volumes. An immense research advancement has been made in the utilization of MOFs since the past 10–15 years [3–5], such as catalysis [6–9], gas storage [10–13] and gas separation [14–18]. Numerous overview or review articles has been published in the last years indicating the increasing interest in MOF chemistry [19–24].

Microporous materials with a high vapor uptake capacity are of increasing interest for low temperature heat transformation applications in thermally driven adsorption chillers (TDCs) or adsorption heat pumps (AHPs). TDCs or AHPs could be an alternative to traditional compressor air conditioners or heat pumps run by electricity or fossil fuels. The use of solar or waste heat as the driving energy in TDCs or AHPs can minimize primary energy consumption. In Fig. A.8 the thermodynamic principle for adsorption chillers or heat pumps is displayed [25–31]. In the case of a cooling application $Q_{evap}$ is used as useful cold and $Q_{ads}$ and $Q_{cond}$ are released to the environment. During a heat pump application $Q_{evap}$ can be delivered from the environment at low temperature and $Q_{ads}$ and $Q_{cond}$ will be useful higher temperature heat. The working fluid is exchanged reversibly between the evaporation/condensation vessel and the porous material where ad- and desorption takes place. Alcohols like methanol or water are suitable, vaporizable working fluids due to their high evaporation enthalpies. Water is often the working fluid of choice because of its high evaporation enthalpy (2440 kJ $kg^{-1}$ at 25 °C) and non-toxicity despite the need to work under vacuum because of the low vapor pressure of only 3.17 kPa at 25 °C. Alcohols like methanol and ethanol are interesting alternatives because of the lower boiling points so that evaporator temperatures below 0 °C are possible [32].

New research developments aim for new porous materials as adsorbents due to disadvantages of classical adsorbents (silica gels, zeolites, aluminophosphates) [33–38]. Zeolites have a high affinity to water and therefore require high desorption temperatures with a not too high water uptake capacity. Silica gels have a lower hydrophilic character than zeolites which leads to lower desorption temperatures but a low water loading lift in the ideal interval $0.05 < P \cdot P_0^{-1} < 0.35$. Hence, MOFs have been studied as adsorbents for cycling vapor sorption (mostly water and methanol) over the last years [33–35,39–50]. MIL-101(Cr) (Fig. A.9) [51–53] is a promising material for potential heat transformation processes with its high BET surface (>3000 $m^2$ $g^{-1}$), the large water and methanol

* Corresponding author. Tel.: +49 2118112286.
*E-mail address:* janiak@uni-duesseldorf.de (C. Janiak).

http://dx.doi.org/10.1016/j.micromeso.2014.11.025
1387-1811/

uptake capacity (>1 g $g^{-1}$) and good cycling stability [40,49]. Besides vapor sorption applications MIL-101(Cr) has been investigated for drug delivery [54], catalysis [55–57] and gas storage [58,59], sometimes in connection with post-synthetic modifications [55,56,59,60].

MOFs are generally obtained as (micro)crystalline powders, which is disadvantageous for potential applications, e.g., due to dust problems. Therefore shaping of MOFs into a mechanically manageable form is an indispensable requirement. Composite materials containing MOFs and an organic component (mostly polymers) can be named "shaped MOFs" and possess the chemical and physical properties of each component. MOF-organic matrix composites are well known as membranes [61–65], fibers [66–68] and as beads [69]. Küsgens and coworkers manufactured a MOF in a monolithic shape in a two-step process: pre-synthesized HKUST-1 crystals were mixed together with a liquid binding agent and a plasticizer followed by extrusion to a monolithic structure [70]. Monolithic HKUST-1@Aerogel composites were synthesized by in-situ HKUST-1 formation in the macropores of a pre-synthesized porous carbon monolith [71–73], or by adding HKUST-1 powder during silica aerogel synthesis [74]. Hierarchical composites of HKUST-1 in macroporous polyacrylamide (PAM) beads, HKUST-1 in macro-/mesoporous silica and UiO-66 in polyurethane (PU) foams were synthesized by Bradshaw, Galarneau and Pinto et al. [69,75,76]. Monolithic structures can also be manufactured based on polymerized high internal phase emulsions, so called poly(HIPEs) [77–79]. Hydrophilic, macroporous poly(HIPEs) are synthesized by concentrated o/w emulsions, where an oily phase (o) is added dropwise to an aqueous solution (w) consisting of a hydrophilic monomer and a crosslinker. The internal, oily phase occupies more than 74% of the volume of the emulsion, kinetically stabilized by a surfactant. After polymerization of the monomer in the aqueous, continuous phase, the organic phase can be removed by washing steps and drying, and a monolithic structure can be obtained. The only MOF@HIPE composite reported, so far, is HKUST-1 which was synthesized in-situ into a pre-formed macroporous HIPE based on 4-vinylbenzyl chloride crosslinked with divinylbenzene [80]. A three-step synthetic route was used to obtain a monolithic HKUST-1@HIPE hybrid material with a maximal BET surface area of 570 $m^2 g^{-1}$ and a pore volume of 0.38 $cm^3 g^{-1}$. The HIPE material then contained 62.3 wt% of HKUST-1 after the third impregnation step. Taking into account the MOF loading and BET surface areas of pure HKUST-1 and HIPE with 1340 $m^2 g^{-1}$ and 30 $m^2 g^{-1}$, respectively, the estimated BET surface area of 846 $m^2 g^{-1}$ could not be achieved. No potential applications, e.g., as gas storage material, were investigated with HKUST-1@HIPE.

In this work we present the embedding of pre-synthesized MIL-101(Cr) crystals into a poly(HIPE) material based on polymerized 2-hydroxyethylmethacrylate (HEMA), crosslinked with *N,N′*-methylenebisacrylamide (MBA) (see Scheme 1) [81,82]. The methanol and water uptake capacities of the MIL-101(Cr)@poly(HEMA)HIPE or in short MIL-101@HIPE composites were investigated.

## 2. Experimental

### 2.1. Materials and methods

All chemicals were obtained commercially and used without further purification except *N,N′*-methylenebisacrylamide (MBA), which was recrystallized from methanol: 2-hydroxyethyl methacrylate (HEMA) (Alfa Aesar 97% stabilized with approx. 500 ppm 4-methoxyphenol), *N,N′*-methylenebisacrylamide (MBA) (Sigma–Aldrich 99%), ammonium persulfate (APS) (Roth ⩾ 98%), Kolliphor® P188 (Sigma), *N,N,N′,N′*-tetramethylethylenediamine (TMEDA) (Merck > 99%), $Cr(NO_3)_3 \cdot 9H_2O$ (Acros Organics 99%), 1,4-benzenedicarboxylic acid ($H_2BDC$) (Acros Organics > 99%), tetramethylammonium hydroxide (TMAOH) (25 wt% in water), cyclohexane (AppliChem. p.a.), DMF (VWR, p.a.), ethanol (VWR, p.a.). All experimental work was performed with exposure to air.

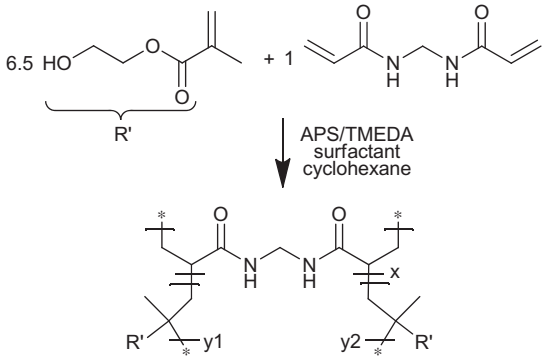


**Scheme 1.** Radical polymerization of 2-hydroxyethyl methacrylate (HEMA) and *N,N′*-methylenebisacrylamide (MBA) initiated by ammonium persulfate (APS) ($x$ = 13 mol-%, $y1 + y2$ = 87 mol-%).

### 2.2. Physical measurements

Powder X-ray diffraction (PXRD) patterns were done at ambient temperature on a Bruker D2 Phaser using a flat sample holder and Cu-Kα radiation ($\lambda$ = 1.54182 Å). FT-Infrared spectra were measured on a Bruker TENSOR 37 IR spectrometer at ambient temperature as KBr disk in the range of 4000–500 $cm^{-1}$. Nitrogen physisorption isotherms were carried out on a Quantachrome Nova 4000e at 77 K. Water and methanol physisorption isotherms were measured volumetrically on a Quantachrome Autosorb iQ MP at 293 K. The materials were put into sample tubes capped with septa. The weighed sample tubes were attached to the preparation port of the sorption analyzer, degased under vacuum (3–4 h at 373–473 K), weighed out again and then transferred to the analysis port of the sorption analyzer. For determination of the cold and warm free space of the sample tubes helium gas was used. DFT calculations for the pore size distribution curves were done with the native NovaWin 11.03 software using the '$N_2$ at 77 K on carbon, slit pore, NLDFT equilibrium' model [83–85]. Scanning electron microscopy images of poly(HEMA)HIPE and pre-polymerized MIL-101@HIPE composites were obtained with a LEO 1430 VP SEM after coating with Au for 180 s at 30 mA by an AGAR sputter coater. MIL-101(Cr) and standard MIL-101@HIPE composites (without pre-polymerization) were imaged on a FEI Quanta 400 FEG (ESEM). Before imaging the materials were coated with Au/Pd (80: 20) using an Emitech K550 sputter for 1 min at 15 mA. The thermogravimetric analysis (TGA) curve of poly(HEMA)HIPE was measured on a TG 209 F3 Tarsus from Netzsch.

### 2.3. Synthesis of MIL-101(Cr)

MIL-101(Cr) was hydrothermally synthesized according to the literature [58]. Typical batch sizes of 4.80 g (12.0 mmol) $Cr(NO_3)_3 \cdot 9H_2O$, 1.98 g (11.9 mmol) $H_2BDC$, 1.1 mL TMAOH (3.1 mmol; $\rho$ = 1.014 g $mL^{-1}$; 25 wt% in $H_2O$) and 60 mL of deionized water at 453 K for 24 h yielded MIL-101(Cr)-as synthesized. For activation the as-synthesized MIL-101 was purified through a consecutive washing procedure with DMF, EtOH and deionized water (see Supplementary data for details). 2.34 g of purified MIL-101 was obtained (50% yield based on Cr) as a green powder with a BET surface of 3060 $m^2 g^{-1}$ and a pore volume of 1.45 $cm^3 g^{-1}$ (measured at $P \cdot P_0^{-1}$ = 0.95), which was calculated from the type-I

$N_2$ sorption isotherm (Fig. A.2a, Table A.1). Experimental, theoretical powder X-ray patterns and the IR-spectrum are shown in Fig. A.1.

### 2.4. Synthesis of poly(HEMA)HIPE

The synthesis of native poly(HEMA)HIPE, from 2-hydroxyethyl methacrylate copolymerized with 13 mol% *N,N′*-methylenebisacrylamide, was carried out according to the literature [81,82]. The reaction equation for the radical polymerization is displayed in Scheme 1. An aqueous solution of the monomer 2-hydroxyethyl methacrylate and copolymer *N,N′*-methylenebisacrylamide was prepared. After adding ammonium persulfate, as the radical initiator and the surfactant Kolliphor® P188 (poly(ethylene glycol)-*block*-poly(propylene glycol)-*block*-poly(ethylene glycol)), cyclohexane as the internal organic phase of the o/w emulsion was slowly added dropwise into the aqueous solution. Addition of *N,N,N′,N′*-tetramethylethylenediamine, which acts together with APS as a redox initiator pair, was necessary for a successful curing of the emulsion. Curing for 3 days at room temperature, followed by washing and drying steps led to a mechanically stable, white monolith (Fig. 3a) (see Supplementary data for details).

### 2.5. Synthesis of MIL-101@HIPE composites

MIL-101@HIPE composites (in short for MIL-101(Cr)@poly(HEMA)HIPEs) with different weight percentages of MIL-101(Cr) were synthesized by a modified synthetic procedure of the pure poly (HEMA)HIPE material. Various amounts of well ground MIL-101 powders were filled in 5 mL plastic syringes, which were cut off from one side (side where the cannula is normally attached). Then specific amounts of pure emulsions were added to each syringe and after homogenization, curing, washing and drying green monoliths were obtained (Fig. 3b). The composites were synthesized in three different ways: (i) standard without and (ii) with additional pre-polymerization (pp) of the HIPE emulsion and (iii) with impregnation of the MIL with cyclohexane ($cC_6$). Modifications (ii) and (iii) are indicated by the prefix pp- and $cC_6$-, respectively, to MIL-101@HIPE. The weight percentages of MIL-101(Cr) in the composites were calculated by simply dividing the amount of MIL added to the HIPE by the final mass of the composites supposing no MOF was lost during the synthesis (see Formula A.1).

## 3. Results and discussion

### 3.1. Pure poly(HEMA)HIPE

Infrared spectroscopic analysis of the HIPE materials supports their purity due to the absence of bands for starting materials like monomers or surfactant (Fig. 1). The region between 3720 and 3140 $cm^{-1}$ shows a broad band which can be assigned to the O–H and N-H stretching vibrations of free water in the pores of the HIPE material and the bonded MBA copolymer respectively. Beside the $\nu$(C–H) stretching vibrations at around 2950 $cm^{-1}$, infrared data shows typical carbonyl stretching vibrations in the region of 1740 and 1640 $cm^{-1}$. Compared to the infrared spectrum of pure poly(HEMA) material without the presence of bonded MBA, the band at 1539 $cm^{-1}$ can be assigned to deformation vibrations of the N–H bond [86,87]. Other characteristic vibration bands like $\delta$(C–H) (1470–1380 $cm^{-1}$), $\nu$(C–O) (1263 $cm^{-1}$), $\nu$(C–N) (1161 $cm^{-1}$), $\nu$(C–O–C) (1078 $cm^{-1}$) and $\gamma_{oop}$(748 $cm^{-1}$) display the presence of the anticipated functional groups.

The porosity of the macroporous poly(HEMA)HIPE material was assessed by $N_2$ sorption experiments (Fig. A.3b) and scanning electron microscopy (Fig. 2). Multi-point BET calculations from the $N_2$ sorption isotherm show a BET surface area of 50 $m^2\ g^{-1}$ (Table A.1). The typical macroporous morphology, which is known for HIPE systems is shown in Fig. 2 [77–79]. The diameters of the voids

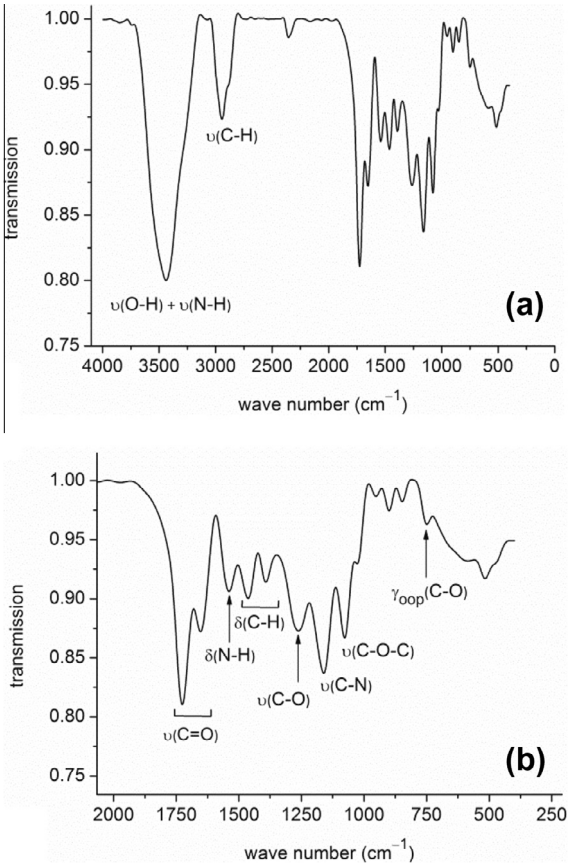


**Fig. 1.** (a) IR-spectrum (KBr) of poly(HEMA)HIPE. (b) Enlargement for region 250–2000 $cm^{-1}$.

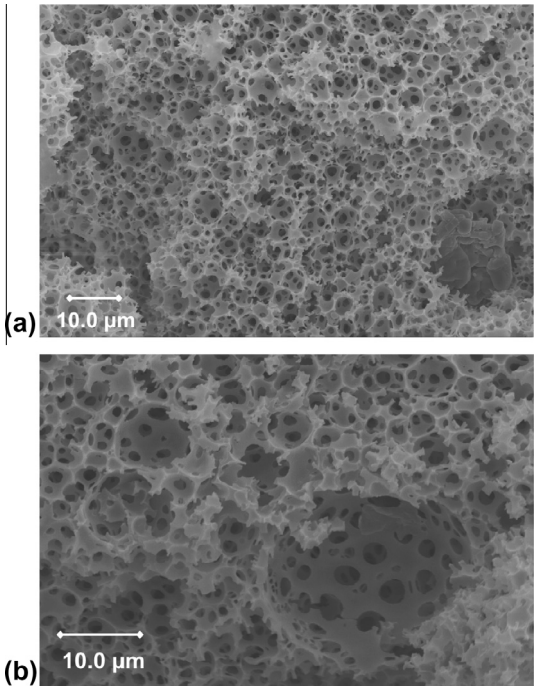


**Fig. 2.** (a)–(b) Scanning electron microscopic (SEM) images of poly(HEMA)HIPE (average pore size diameter 2–6 µm).

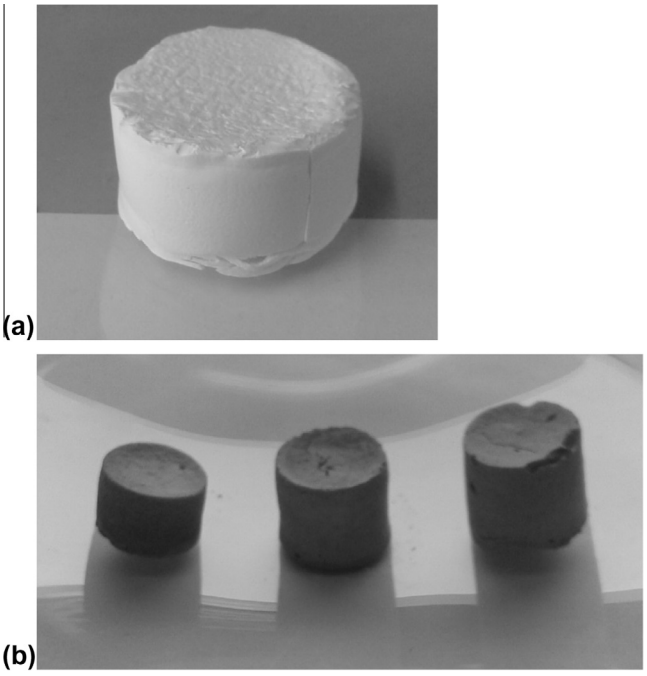


**Fig. 3.** (a) Pure poly(HEMA)HIPE material. (b) pp-MIL-101@HIPE composites with 38, 59 and 67 wt% of MIL-101. Dimensions are for (a) 22 × 15 mm, and for (b) 13 × 11, 13 × 14, 13 × 17 mm. The first values stand for the diameter, the second for the height.

and the connecting pores of 2–6 μm and 1–2 μm are consistent with other literature data [81,82]. It has to be mentioned that porosity analysis of such macroporous systems should better be evaluated from mercury intrusion porosimetry experiments, which is the favored method for the analysis of macropores between 3 nm and 950 μm. Porosity analysis based on gas physisorption is limited to pore sizes with diameter of 400 nm and below. The pore size distribution curve of poly(HEMA)HIPE, calculated from mercury intrusion measurements, was taken from the literature and displayed in Fig. A.4d. The only pore size of approximately 1.0(±0.1) μm, found by mercury porosimetry, is consistent with the SEM image reflecting the size of the connecting pores [81].

### *3.2. Embedding MIL-101(Cr) into poly(2-hydroxyethyl methacrylate) monoliths*

By modifying the synthetic procedure for crosslinked poly(HEMA)HIPEs through addition of specific amounts of emulsion to selected amounts of MIL powders, green monoliths with 38, 59 and 67 wt% of MIL-101(Cr) can be obtained (Fig. 3b, see Formula S1 for definition of wt%). MIL-101@HIPE with 67 wt% of MIL turned out to be mechanically not stable enough, which means that it crumbled easily due to the high amount of MIL-101 powder. The monolithic composites were synthesized in three different ways: (i) as standard the HIPE emulsions were added to the MILs after a short period of stirring, that is, without pre-polymerization (38, 59 and 67 wt% MIL in MIL-101@HIPE), (ii) after a longer pre-stirring time, that is, with pre-polymerization (38 and 59 wt% MIL in pp-MIL-101@HIPE) and (iii) with impregnation of the MIL with cyclohexane before adding the HIPE emulsions (38 and 59 wt% MIL in $cC_6$-MIL-101@HIPE). The last two ways of synthesis have been carried out in order to avoid pore blocking by HIPE-monomer polymerization in the MIL pores. The stirring time of the HIPE emulsion was elongated in (ii), which is equivalent to a HIPE pre-polymerization. This should lower the diffusion rate of HIPE-monomers/oligomers into the MIL pores. Another way of protecting the MIL pores utilized the insolubility of HEMA and MBA

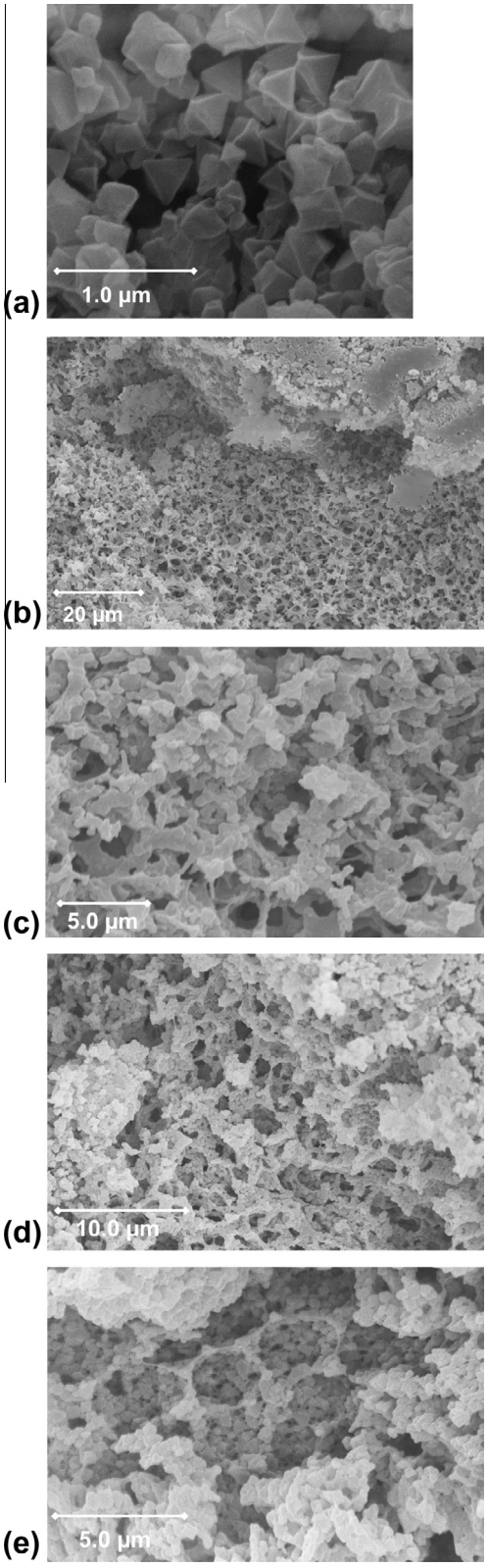


**Fig. 4.** Scanning electron microscopic (SEM) images of (a) MIL-101(Cr) and pp-MIL-101@HIPE composites with (b)–(c) 38 wt% and (d)–(e) 59 wt% of MIL-101.

monomers in cyclohexane. Therefore, in (iii) the MIL powders were impregnated with cyclohexane before adding HIPE emulsions to protect the pores from intrusion by HEMA/MBA-monomers (see Supplementary data for details).

Scanning electron images of pure MIL-101(Cr) show the typical octahedral morphology with a particle size varying between 300 and 500 nm, typical for hydrothermally synthesized MIL-101(Cr) (Fig. 4a) [58]. Fig. 4b–e shows the composite materials with 38 and 59 wt% loading of MIL-101(Cr) (pp-MIL-101@HIPE). Fig. 4b shows HIPE voids with an almost unchanged diameter. The MIL particles adhere on the HIPE walls mostly as agglomerates. MIL octahedrons, which seem to have an unchanged particle size, can be found in the agglomerates (Fig. 4c). The higher loading of MIL-101(Cr) is apparent in the SEM images by simply comparing Fig. 4b, c with 6d, e. Even at a high MIL loading of 59 wt% the original HIPE morphology with its macroscopic voids is still evident (Fig. 4d–e). The adherence of particles to the HIPE walls and not occupying the voids was also shown for a polystyrene coated poly(NIPAM)HIPE (NIPAM: *N*-isopropylacrylamide) [88]. Similar SEM images with 38 and 67 wt% of MIL-101(Cr) in MIL-101(Cr)@poly(HEMA)HIPE (standard procedure) are displayed in Fig. A.5b–f.

The powder X-ray diffraction patterns of the composite compounds standard- and pp-MIL-101@HIPE with 38, 59 and 67 wt% of MIL show that the crystallinity remains unchanged compared to pure MIL-101(Cr) (Fig. 5a).

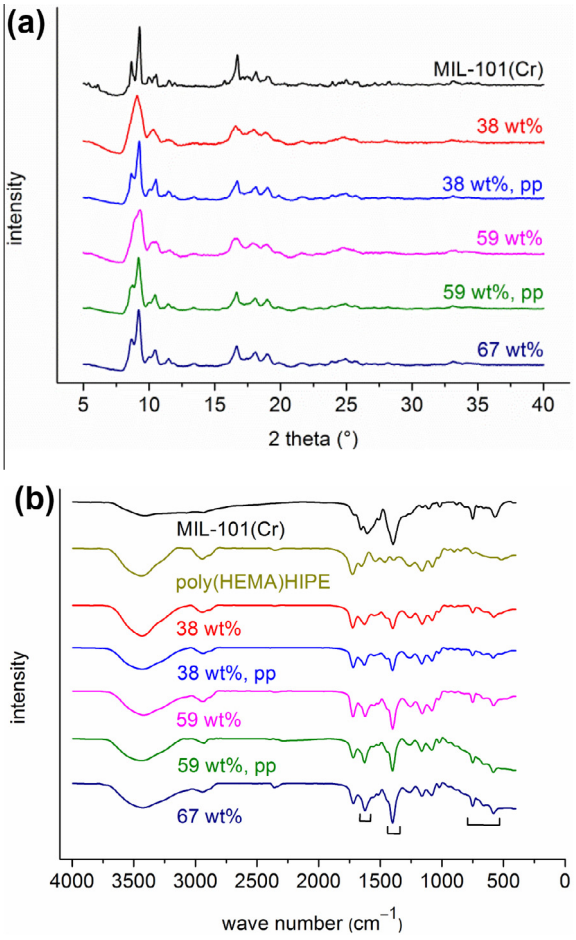


**Fig. 5.** (a) Experimental powder X-ray diffraction pattern of activated MIL-101(Cr) standard- and pp-MIL-101@HIPE composites with 38, 59 and 67 wt% of MIL. (b) IR-spectra (KBr) of activated MIL-101(Cr), poly(HEMA)HIPE, standard- and pp-MIL-101@HIPE composites with 38, 59 and 67 wt% of MIL-101. Square brackets highlight the bands of MIL-101 in the composite materials.

Infrared spectra of the composites can be seen as an overlap of the individual spectra of MIL-101(Cr) and poly(HEMA)HIPE (Fig. 5b). With increasing loading of the MIL the intensities of the characteristic vibration bands for MIL-101 in the composite materials are enhanced (see regions highlighted by square brackets in Fig. 5b).

### 3.3. $N_2$, *methanol and water sorption studies*

Fig. 6a shows the $N_2$ sorption isotherms of the standard- and pp-MIL-101@HIPE composites in comparison to the pure poly(HEMA)HIPE. As expected an increasing amount of MIL-101 in MIL-101@HIPE leads to higher nitrogen adsorption and BET surface areas (Table 1). Importantly, the $N_2$ uptake and BET surface area increase significantly for the same MIL wt% upon pre-polymerization (pp) of the poly(HEMA)HIPE compared to the standard procedure without pre-polymerization. For example, for 59 wt% the BET surface is 990 $m^2 g^{-1}$ for the pre-polymerized pp- and only 450 $m^2 g^{-1}$ for standard MIL-101@HIPE (Table 1). The $N_2$ sorption isotherms are consistent with type-I isotherms therefore proving the accessibility of nitrogen to the micropores of MIL-101 (Fig. A.2c). Yet, the characteristic shape of the $N_2$ sorption isotherm of pure MIL-101(Cr) with defined steps between $0.1 < P \cdot P_0^{-1} < 0.2$ (Fig. A.2a), which are attributed to two kinds of mesopores (Fig. A.9), is not well developed in the MIL@HIPE composites [51]. The almost negligible steps between $0.1 < P \cdot P_0^{-1} < 0.2$ in the composites are explained by the overall lower $N_2$ uptake of 1/3 and less due to the decrease in surface area in the composites.

Pore size distribution curves show that pure MIL-101(Cr) possesses different pores in the micro- and mesoporous area

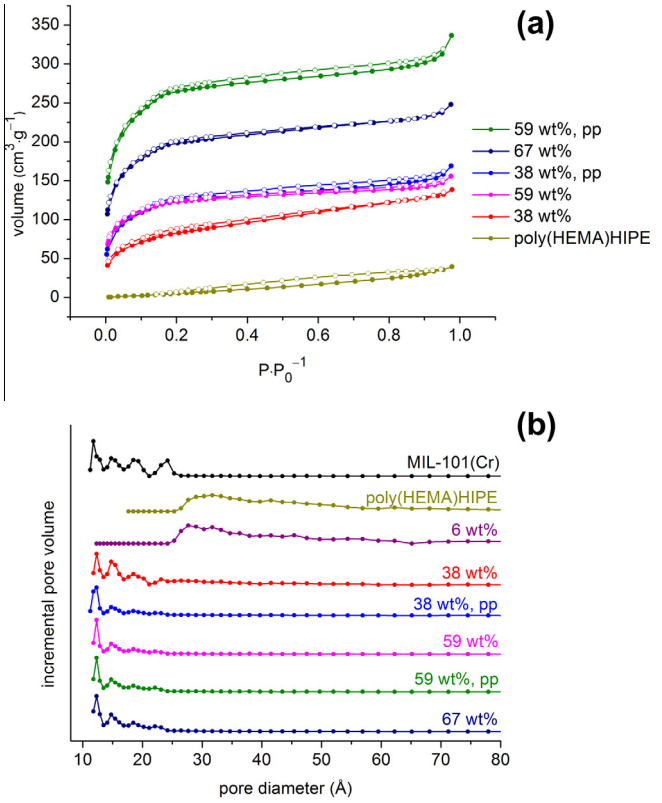


**Fig. 6.** (a) $N_2$-sorption isotherms of standard- and pp-MIL-101@HIPE composites with 38, 59 and 67 wt% MIL-101(Cr). (b) Pore size distribution curves of activated MIL-101(Cr), poly(HEMA)HIPE, standard- and pp-MIL-101@HIPE composites with 6, 38, 59 and 67 wt% MIL-101(Cr). Adsorption is depicted with filled, desorption with empty symbols (degassing conditions: 4 h, 373 K).

**Table 1**
Nitrogen, methanol and water sorption measurements of poly(HEMA)HIPE and composite materials.

| Materials | BET surface area [a]; (Estimated) [b] ($m^2 \cdot g^{-1}$) | Water loading [c]; (Estimated) [d] ($g \cdot g^{-1}$) | Methanol loading [c]; (Estimated) [d] ($g \cdot g^{-1}$) |
|---|---|---|---|
| poly(HEMA)HIPE | 50 | 0.16 | 0.30 |
| MIL-101(Cr) | 3060 | 1.06 | 1.08 |
| Composites: [e] | | | |
| 6 wt% | 30 (230) | n.d. | n.d. |
| 38 wt% | 300 (1190) | n.d. | n.d. |
| 38 wt%, pp | 460 (1190) | 0.21 (0.50) | 0.33 (0.60) |
| 38 wt%, $cC_6$ | 290 (1190) | n.d. | n.d. |
| 59 wt% | 450 (1830) | n.d. | n.d. |
| 59 wt%, pp | 990 (1830) | 0.29 (0.69) | 0.37 (0.76) |
| 59 wt%, $cC_6$ | 450 (1830) | n.d. | n.d. |
| 67 wt% | 540 (2050) | n.d. | n.d. |

[a] BET surface area calculated at $0.05 < P \cdot P_0^{-1} < 0.2$ from $N_2$ sorption isotherm 77 K with a standard deviation ± 20 $m^2\ g^{-1}$.
[b] BET surface area as the sum of the mass-weighted surface areas of MIL-101(Cr) (3060 $m^2\ g^{-1}$) and HIPE (50 $m^2\ g^{-1}$) calculated from the following formula:

$$\text{BET(estimated)} = \frac{\text{wt\% of MIL} - 101\text{(Cr)}}{100} \times 3060\ \text{m}^2\ \text{g}^{-1} + \frac{\text{wt\% of MIL}}{100} \times\ 50\ \text{m}^2\ \text{g}^{-1}$$

[c] Calculated from water sorption isotherm at 293 K ($P \cdot P_0^{-1} = 0.9$). n.d. = not determined.
[d] Water and methanol loading estimated as the sum of the mass-weighted vapor uptakes at $P \cdot P_0^{-1} = 0.9$ of MIL-101(Cr) (1.06 g $g^{-1}$ for water; 1.08 g $g^{-1}$ for methanol) and HIPE (0.16 g $g^{-1}$ for water; 0.30 g $g^{-1}$ for methanol) calculated from the following formula:

$$\text{Vapor loading(estimated)} = \frac{\text{wt\% of MIL} - 101\text{(Cr)}}{100} \times 1.06\ \text{(water) or } 1.08\ \text{(methanol) g g}^{-1} + \frac{\text{wt\% of HIPE}}{100} \times 0.16\ \text{(water) or } 0.30\ \text{(methanol) g g}^{-1}$$

[e] wt% refers to MIL-101(Cr) amount.

(Fig. 6b). The two maxima at diameters 12 and 15 Å could be assigned to the regions of the pentagonal and hexagonal windows, which surround the actual pores with 19 and 24 Å in diameter (see Fig. A.9). Compared to literature data these two pores are smaller than expected (29 and 34 Å) possibly due to retained impurities of unreacted $H_2$BDC ligand located in the pores [20]. The pore size distribution curves of the composites show that the micro- and mesopores, especially the pores with 12 and 15 Å in diameter, remain unchanged therefore proofing the accessibility for nitrogen (Fig. 6b).

From the wt% of MIL-101(Cr) in the composite the BET surface areas could be estimated (expected) as the sum of the mass-weighted surface areas of pure MIL and HIPE (see Table 1 for further explanation). Synthesizing the composites by the standard procedure (MIL-101@HIPE) led to BET surface areas, which are approximately four times lower compared to the expected BETs (Table 1). A possible explanation would be that 75% of the pores of MIL-101(Cr) in the composites are fully blocked by HIPE material and only 25% of pores are still accessible. To confirm the assumption that the HIPE material is able to fully block the pores of MIL-101(Cr) a composite material was synthesized with only 6 wt% of MIL-101 (see Supplementary data for details). Offering a large excess of HIPE over the MIL amount could be expected to result in full blockage of the pores of MIL-101(Cr). The BET surface area and pore size distribution of the 6 wt% MIL loaded composite material match those of the pure HIPE material. Hence, it is apparent that a sufficient excess of poly(HEMA)HIPE material is indeed able to block all MIL pores (Table 1, Fig. 6b).

In order to avoid or minimize pore blocking by HIPE polymerization in the pores of MIL-101, which occurs to a great extent in the standard procedure (i), the monolithic composites were also synthesized in two other ways; (ii) after a longer pre-stirring time, that is, with pre-polymerization and (iii) with impregnation of the MIL with cyclohexane before adding the HIPE emulsions. (ii) Increasing the stirring time of the HIPE emulsion is equivalent to a higher degree of HIPE polymerization. HEMA and MBA monomers were pre-polymerized to create longer oligomers and polymer chains, which are more hindered to diffuse into the MIL-101 pores. The BET surface areas could indeed be increased from 300 to 460 $m^2\ g^{-1}$ for 38 wt% MIL-101@HIPE and from 450 to 990 $m^2\ g^{-1}$ for 59 wt% MIL-101@HIPE upon pre-polymerization (Table 1). This shows that pre-polymerization is an indispensable step for MIL-101@poly(HEMA)HIPE syntheses to create monoliths with maximized porosities (see Supplementary data for details). Still, the expected BET surface areas of 1190 $m^2\ g^{-1}$ (38 wt%) and 1830 $m^2\ g^{-1}$ (59 wt%) could not be achieved showing that total protection of the MIL micro- and mesopores by pre-polymerization is not possible (Table 1). (iii) Impregnating the MIL-101(Cr) pow-

ders with cyclohexane before adding the HIPE emulsion should fill and protect the MIL pores from HIPE polymerization due to the insolubility of HEMA and MBA monomers in cyclohexane. Unfortunately this approach did not lead to increased BET surface areas compared to the standard procedure (Table 1, Fig. A.6).

This phenomenon of not achieving the estimated BET surface areas is literature-known. Similar hierarchical composites like HKUST-1 embedded in porous carbon monoliths only reach approx. 40% of the calculated BET surface areas [73]. Other composites like UiO-66@polyurethane or HKUST-1@HIPE reach about 60% of the theoretically estimated values [76,80]. Our 38 wt% and 59 wt% loaded pp-MIL-101@HIPE composites lie also in this range. MOFs in inorganic templates, like HKUST-1 embedded in silica aerogels [74] or HKUST-1@macro-/mesoporous silica [75] match or even exceed the estimated BET values (Table A.3). We note that the MOF wt% determination in the composite HKUST-1@PAM was based on a BET surface area determination under the assumption that 100% of the native MOF surface area will be retained and still accessible in the composite [69]. However, from other and our study of MOF composites with organic polymers it is evident that the organic matrix leads to partial pore blocking.

For investigation of the hydrophilicity of the pure poly(HEMA)-HIPE and interactions between vapor and native adsorbent, methanol and water vapor were tested as possible working fluids. It has been shown that methanol is the more suitable vapor showing almost twice the amount of total vapor uptake toward pure poly(HEMA)HIPE. 0.30 g g$^{-1}$ of methanol and 0.16 g g$^{-1}$ of water vapor are adsorbed at $P \cdot P_0^{-1} = 0.9$ (Fig. 7, Table 1). Therefore pure poly(HEMA)HIPE is rather hydrophobic.

Water and methanol sorption isotherms of pp-MIL-101@HIPE with 38 and 59 wt% loading are shown in comparison to the sorption isotherm of the pure MIL and poly(HEMA)HIPE in Fig. 8. The higher uptake capacities (Table 1) compared to the pure HIPE is apparent for both vapors. The maximum water loadings of the 38 and 59 wt% composite materials are 0.21 and 0.29 g g$^{-1}$, respectively, at $P \cdot P_0^{-1} = 0.9$ and higher than the loading of pure poly(HEMA)HIPE with 0.16 g g$^{-1}$. Methanol sorption measurements outperform the water uptake capacities with loadings of 0.33 and 0.37 g g$^{-1}$ for both composites together with a steeper adsorption rise up to $P \cdot P_0^{-1} = 0.35$. Gravimetric vapor loading capacities of the composites are comparable to commercial adsorbents like zeolites [34]. Zeolite-like crystalline aluminophosphates (AlPO) and silica-aluminophosphates (SAPO) can provide a higher maximum water uptake capacity than zeolites. For zeolites the strong hydrophilicity significantly reduces the fluid exchange within the cycle for desorption temperatures below 140 °C [28]. AlPOs and SAPOs

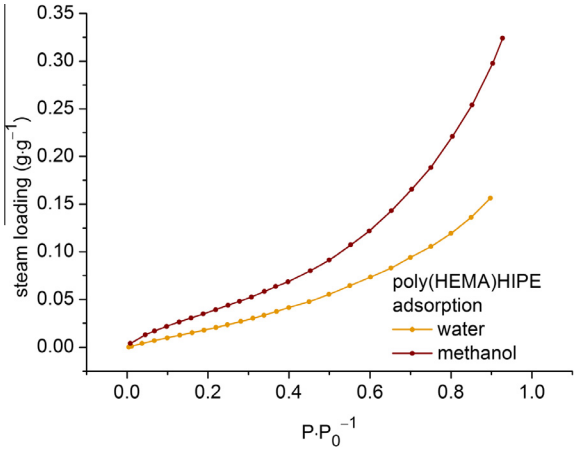


**Fig. 7.** Water and methanol adsorption isotherms of poly(HEMA)HIPE.

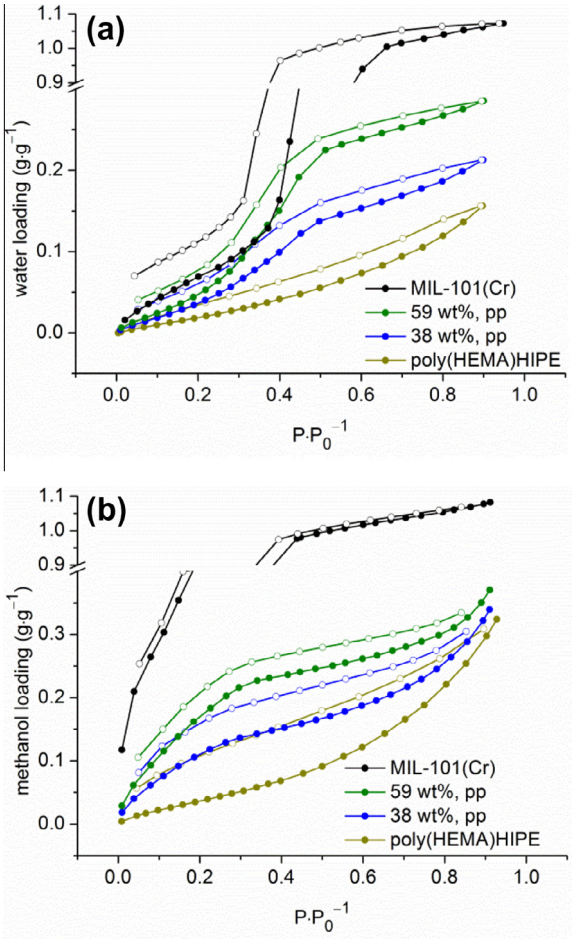


**Fig. 8.** (a) Water and (b) methanol sorption isotherms of poly(HEMA)HIPE, MIL-101(Cr) and pp-MIL-101@HIPE composites with 38 and 59 wt% MIL-101(Cr). Adsorption is depicted with filled, desorption with empty symbols.

have the desired s-shape adsorption isotherms for water uptake. Yet, the broader use of AlPOs and SAPOs for heat transformations is hampered by the high costs of the solvothermal/hydrothermal syntheses which requires the use of (expensive) template molecules or salts, such as morpholine or tetramethylammonium hydroxide [49].

The expected vapor loading at $P \cdot P_0^{-1} = 0.9$ can be estimated from maximum vapor loadings of poly(HEMA)HIPE and MIL-101(Cr) taking into account their wt% in the composite material (Table 1). The lower than estimated vapor uptake correlates with the lower than estimated BET surface area of the composites. Again, methanol is the more suitable working fluid because the experimental vapor uptake capacities are closer to the estimated values (Table 1). The lower fraction of water uptake of MIL-101@HIPE to pure MIL-101 corresponds rather well to the lower surface fraction. For example, 59% MIL-101@HIPE has about one third of the BET surface of MIL-101 (990/3060) and exhibits about one third of the water uptake capacity (0.29/1.06).

A sorption material for TDCs or AHPs should show a high water uptake capacity at low to medium humidity and desorb the vapor at low temperature (below 80 °C) [89]. Ideally, a porous material should perform in between $0.05 < P \cdot P_0^{-1} < 0.35$ relative pressure range with a sharp, s-shaped loading step and should have a desorption temperature at or below 80 °C [33,90].

To check if longer diffusion paths through the monolith could have influenced the gas adsorption the MIL-101@HIPE monoliths

were measured again as well ground powders and with a longer equilibration time for the adsorption points of the isotherms. However, almost unchanged BET surface areas were obtained from nitrogen adsorption (Table A.2). Thus, the accessibility of nitrogen to the pores of the composite materials seems to be independent from the shape or diffusion path length.

## 4. Conclusion

We presented the successfully embedding of the micro- and mesoporous metal-organic framework MIL-101(Cr) into a macroporous, high internal phase emulsion (HIPE) foam based on cross-linked poly(2-hydroxyethyl methacrylate) by simply adding the high internal phase emulsion to the MOF before curing. The MIL-101(Cr)@poly(HEMA)HIPE composites (in short MIL-101@HIPEs) were characterized by X-ray powder diffraction, IR-spectroscopy, scanning electron microscopy, nitrogen- methanol and water sorption studies. A maximal loading of 59 wt% MIL was achieved with a mechanically stable monolithic shape. Pre-polymerization of the HIPE emulsions was shown to be an indispensable factor for synthesizing highly porous composites where the micro- and mesopores of MIL-101(Cr) remain partially unblocked. As seen before for HKUST-1@porous carbon [73], UiO-66@polyurethane [76] and HKUST-1@HIPE [80] the BET surfaces of MIL-101@HIPE composites are lower than expected from the MOF weight percentage. Still, the MIL-101@HIPE monoliths show higher methanol and water uptake capacities compared to the pure HIPE. The maximum vapor exchange of 0.29 g $g^{-1}$ (for water) and 0.37 g $g^{-1}$ (for methanol) of the MIL-101@HIPE composite is certainly lower than in pure MIL-101(Cr) but most of it can be utilized under realistic working conditions up to $P \cdot P_0^{-1} = 0.4$. Embedding of other water-stable MOFs like MIL-100(Fe) and MIL-100(Cr) will be investigated.

## Acknowledgements

Support by the University of Düsseldorf through its strategic research fund (SFF) is gratefully acknowledged. We thank Mr. Steffen Köhler for help with the SEM images.

## Appendix A. Supplementary data

Supplementary data associated with this article can be found, in the online version, at http://dx.doi.org/10.1016/j.micromeso.2014.11.025.

## References

[1] O.M. Yaghi, H. Li, J. Am. Chem. Soc. 117 (1995) 10401–10402.
[2] O.M. Yaghi, G. Li, H. Li, Nature 378 (1995) 703–705.
[3] J.R. Long, O.M. Yaghi, Chem. Soc. Rev. 38 (2009) 1213–1214.
[4] S. Kitagawa, S. Natarajan, Eur. J. Inorg. Chem. 24 (2010) 3685.
[5] C. Serre, S. Kitagawa, P.D.C. Dietzel, Micropor. Mesopor. Mater. 157 (2012) 1–2.
[6] M. Yoon, R. Srirambalaji, K. Kim, Chem. Rev. 112 (2012) 1196–1231.
[7] D. Farrusseng, S. Aguado, C. Pinel, Angew. Chem. Int. Ed. 48 (2009) 7502–7513.
[8] J. Lee, O.K. Farha, J. Roberts, K.A. Scheidt, S.T. Nguyen, J.T. Hupp, Chem. Soc. Rev. 38 (2009) 1450–1459.
[9] F.X. Llabrés i Xamena, F.G. Cirujano, A. Corma, Micropor. Mesopor. Mater. 157 (2012) 112–117.
[10] R.B. Getman, Y.-S. Bae, C.E. Wilmer, R.Q. Snurr, Chem. Rev. 112 (2012) 703–723.
[11] Z. Chen, S. Xiang, H.D. Arman, P. Li, S. Tidrow, D. Zhao, B. Chen, Eur. J. Inorg. Chem. 24 (2010) 3745–3749.
[12] F. Ma, S. Liu, D. Liang, G. Ren, C. Zhang, F. Wei, Z. Su, Eur. J. Inorg. Chem. 24 (2010) 3756–3761.
[13] L. Wu, M. Xue, S.-L. Qiu, G. Chaplais, A. Simon-Masseron, J. Patarin, Micropor. Mesopor. Mater. 157 (2012) 75–81.
[14] Z. Zhang, Y. Zhao, Q. Gong, Z. Li, J. Li, Chem. Commun. 49 (2013) 653–661.
[15] J.-R. Li, Y. Ma, M.C. McCarthy, J. Sculley, J. Yu, H.-K. Jeong, P.B. Balbuena, H.-C. Zhou, Coord. Chem. Rev. 155 (2011) 1791–1823.
[16] J.-R. Li, J. Sculley, H.-C. Zhou, Chem. Rev. 112 (2012) 869–932.
[17] Z.R. Herm, R. Krishna, J.R. Long, Micropor. Mesopor. Mater. 157 (2012) 94–100.
[18] M.G. Plaza, A.F.P. Ferreira, J.C. Santos, A.M. Ribeiro, U. Müller, N. Trukhan, J.M. Loureiro, A.E. Rodrigues, Micropor. Mesopor. Mater. 157 (2012) 101–111.
[19] C. Janiak, Dalton Trans. 14 (2003) 2781–2804.
[20] C. Janiak, J.K. Vieth, New J. Chem. 34 (2010) 2366–2388.
[21] G. Férey, Chem. Soc. Rev. 37 (2008) 191–214.
[22] N. Stock, S. Biswas, Chem. Rev. 112 (2012) 933–969.
[23] (a) S. Kitagawa, R. Kitaura, S. Noro, Angew. Chem. Int. Ed. 43 (2004) 2334–2375;
(b) S. Kitagawa, R. Kitaura, S. Noro, Angew. Chem. 116 (2004) 2388–2430.
[24] M. Gaab, N. Trukhan, S. Maurer, R. Gummaraju, U. Müller, Micropor. Mesopor. Mater. 157 (2012) 131–136.
[25] Yu.I. Aristov, Appl. Therm. Eng. 42 (2012) 18–24.
[26] Yu.I. Aristov, J. Chem. Eng. Jpn. 40 (2007) 1242–1251.
[27] A. Hauer, Adsorption 13 (2007) 399–405.
[28] S.K. Henninger, F. Jeremias, H. Kummer, P. Schossig, H.-M. Henning, Energy Procedia 30 (2012) 279–288.
[29] H. Demira, M. Mobedi, S. Ülkü, Renewable Sustainable Energy Rev. 12 (2008) 2381–2403.
[30] Yu.I. Aristov, B. Dawoud, I.S. Glaznev, A. Elyas, Int. J. Heat Mass Transfer 51 (2008) 4966–4972.
[31] H.-M. Henning, Appl. Therm. Eng. 27 (2007) 1734–1749.
[32] L.W. Wang, R.Z. Wang, R.G. Oliveira, Renewable Sustainable Energy Rev. 13 (2009) 518–534.
[33] S.K. Henninger, F. Jeremias, H. Kummer, C. Janiak, Eur. J. Inorg. Chem. 16 (2012) 2625–2634.
[34] C. Janiak, S.K. Henninger, Chimia 67 (2013) 419–424.
[35] Y.-K. Seo, J.W. Yoon, J.S. Lee, Y.K. Hwang, C.-H. Jun, J.-S. Chang, S. Wuttke, P. Bazin, A. Vimont, M. Daturi, S. Bourrelly, P.L. Llewellyn, P. Horcajada, Adv. Mater. 24 (2012) 806–810.
[36] T. Núñez, W. Mittelbach, H.-M. Henning, Appl. Therm. Eng. 27 (2007) 2205–2212.
[37] J. Jänchen, D. Ackermann, H. Stach, W. Brösicke, Sol. Energy 76 (2004) 339–344.
[38] E.-P. Ng, S. Mintova, Micropor. Mesopor. Mater. 114 (2008) 1–26.
[39] P. Küsgens, M. Rose, I. Senkovska, H. Fröde, A. Henschel, S. Siegle, S. Kaskel, Micropor. Mesopor. Mater. 120 (2009) 325–330.
[40] J. Ehrenmann, S.K. Henninger, C. Janiak, Eur. J. Inorg. Chem. 4 (2011) 471–474.
[41] F. Jeremias, A. Khutia, S.K. Henninger, C. Janiak, J. Mater. Chem. 22 (2012) 10148–10151.
[42] S.K. Henninger, H.A. Habib, C. Janiak, J. Am. Chem. Soc. 131 (2009) 2776–2777.
[43] G. Akiyama, R. Matsuda, S. Kitagawa, Chem. Lett. 39 (2010) 360–361.
[44] G. Akiyama, R. Matsuda, H. Sato, A. Hori, M. Takata, Micropor. Mesopor. Mater. 157 (2012) 89–93.
[45] C. Janiak, S.K. Henninger, Nachr. Chem. 61 (2013) 520–523.
[46] A. Khutia, H.U. Rammelberg, T. Schmidt, S. Henninger, C. Janiak, Chem. Mater. 25 (2013) 790–798.
[47] F. Jeremias, V. Lozan, S.K. Henninger, C. Janiak, Dalton Trans. 42 (2013) 15967–15973.
[48] M. Wickenheisser, F. Jeremias, S.K. Henninger, C. Janiak, Inorg. Chim. Acta 407 (2013) 145–152.
[49] F. Jeremias, D. Fröhlich, C. Janiak, S. Henninger, New J. Chem. 38 (2014) 1846–1852.
[50] F. Jeremias, D. Fröhlich, C. Janiak, S.K. Henninger, RSC Adv. 4 (2014) 24073–24082.
[51] G. Férey, C. Mellot-Draznieks, C. Serre, F. Millange, J. Dutour, Science 309 (2005) 2040–2042.
[52] G. Férey, Dalton Trans. 23 (2009) 4400–4415.
[53] G. Férey, C. Serre, Chem. Soc. Rev. 38 (2009) 1380–1399.
[54] P. Horcajada, C. Serre, M. Vallet-Regi, M. Sebban, F. Taulelle, G. Férey, Angew. Chem. 118 (2006) 6120–6124.
[55] Y.K. Hwang, D.Y. Hong, J.-S. Chang, S.H. Jhung, Angew. Chem. 120 (2008) 4212–4216.
[56] D.Y. Hong, Y.K. Hwang, C. Serre, G. Férey, J.-S. Chang, Adv. Funct. Mater. 19 (2009) 1537–1552.
[57] A. Herbst, A. Khutia, C. Janiak, Inorg. Chem. 53 (2014) 7319–7333.
[58] J. Yang, Q. Zhao, J. Li, J. Dong, Micropor. Mesopor. Mater. 130 (2010) 174–179.
[59] A. Khutia, C. Janiak, Dalton Trans. 43 (2014) 1338–1347.
[60] S. Bernt, V. Guillerm, C. Serre, N. Stock, Chem. Commun. 47 (2011) 2838–2840.
[61] E.V. Perez, K.J. Jr., J. Membr. Sci. 328 (2009) 165–173.
[62] S. Basu, A. Cano-Odena, I.F.J. Vankelecom, J. Membr. Sci. 362 (2010) 478–487.
[63] S. Basu, M. Maes, A. Cano-Odena, L. Alearts, D.E. De Vos, I.F.J. Vankelecom, J. Membr. Sci. 344 (2009) 190–198.
[64] H.B. Tanh Jeazet, C. Staudt, C. Janiak, Chem. Commun. 48 (2012) 2140–2142.
[65] H.B. Tanh Jeazet, T. Koschine, C. Staudt, K. Raetzke, C. Janiak, Membranes 3 (2013) 331–353.
[66] R. Ostermann, J. Cravillon, C. Weidmann, M. Wiebcke, B.M. Smarsly, Chem. Commun. 47 (2011) 442–444.
[67] M. Rose, B. Bohringer, M. Jolly, R. Fischer, S. Kaskel, Adv. Eng. Mater. 13 (2011) 356–360.
[68] P. Küsgens, S. Siegle, S. Kaskel, Adv. Eng. Mater. 11 (2009) 93–95.
[69] L.D. O'Neill, H. Zhang, D.J. Bradshaw, J. Mater. Chem. 20 (2010) 5720–5726.
[70] P. Küsgens, A. Zgaverdea, H.-G. Fritz, S. Siegle, S. Kaskel, J. Am. Ceram. Soc. 93 (2010) 2476–2479.
[71] N. Hüsing, U. Schubert, Angew. Chem. 110 (1998) 22–47.
[72] S.A. Al-Muhtaseb, J.A. Ritter, Adv. Mater. 15 (2003) 101–114.

[73] D. Qian, C. Lei, G.-P. Hao, W.-C. Li, A.-H. Lu, Appl. Mater. Interfaces 4 (2012) 6125–6132.
[74] Z. Ulker, I. Erucar, S. Keskin, C. Erkey, Micropor. Mesopor. Mater. 170 (2013) 352–358.
[75] A. Sachse, R. Ameloot, B. Coq, F. Fajula, B. Coasne, D. De Vos, A. Galarneau, Chem. Commun. 48 (2012) 4749–4751.
[76] M.L. Pinto, S. Dias, J. Pires, Appl. Mater. Interfaces 5 (2013) 2360–2363.
[77] N.R. Cameron, Polymer 46 (2005) 1439–1449.
[78] H. Zhang, A.I. Cooper, Soft Matter 1 (2005) 107–113.
[79] N. Brun, S. Ungureanu, H. Deleuze, R. Backov, Chem. Soc. Rev. 40 (2011) 771–788.
[80] M.G. Schwab, I. Senkovska, M. Rose, M. Koch, J. Pahnke, G. Jonschker, S. Kaskel, Adv. Eng. Mater. 10 (2008) 1151–1155.
[81] S. Kovačič, D. Štefanec, P. Krajnc, Macromolecules 40 (2007) 8056–8060.
[82] O. Kulygin, M.S. Silverstein, Soft Matter 3 (2007) 1525–1529.
[83] L.D. Gelb, K.E. Gubbins, R. Radhakrsihan, M. Sliwinska-Bartowiak, Rep. Prog. Phys. 62 (1999) 1573–1659.
[84] N.A. Sedron, J.P.R.B. Walton, N. Quirke, Carbon 27 (1989) 853–861.
[85] A. Vishnyakov, P. Ravikovitch, A.V. Neimark, Langmuir 16 (2000) 2311–2320.
[86] S. Morita, K. Kitagawa, Y. Ozaki, Vib. Spectrosc. 51 (2009) 28–33.
[87] T.S. Perova, J.K. Vij, H. Xu, Colloid Polym. Sci. 275 (1997) 323–332.
[88] N.C. Grant, A.I. Cooper, H. Zhang, Appl. Mater. Interfaces 2 (2010) 1400–1406.
[89] S.K. Henninger, G. Munz, K.-F. Ratzsch, P. Schossig, Adsorption 17 (2011) 833–843.
[90] Yu.I. Aristov, Appl. Phys. Lett. 91 (2007) 111902-1–111902-3.